

A YEE-LIKE FINITE-ELEMENT SCHEME FOR MAXWELL'S EQUATIONS ON UNSTRUCTURED GRIDS

B. RADU[†] AND H. EGGER^{†,*}

[†]*Johann Radon Institute for Computational and Applied Mathematics, Linz, Austria*

^{*}*Institute for Computational Mathematics, Johannes-Kepler University Linz, Austria*

ABSTRACT. A novel finite element scheme is studied for solving the time-dependent Maxwell's equations on unstructured grids efficiently. Similar to the traditional Yee scheme, the method has one degree of freedom for most edges and a sparse inverse mass matrix. This allows for an efficient realization by explicit time-stepping without solving linear systems. The method is constructed by algebraic reduction of another underlying finite element scheme which involves two degrees of freedom for every edge. Mass-lumping and additional modifications are used in the construction of this method to allow for the mentioned algebraic reduction in the presence of source terms and lossy media later on. A full error analysis of the underlying method is developed which by construction also carries over to the reduced scheme and allows to prove convergence rates for the latter. The efficiency and accuracy of both methods are illustrated by numerical tests. The proposed schemes and their analysis can be extended to structured grids and in special cases the reduced method turns out to be algebraically equivalent to the Yee scheme. The analysis of this paper highlights possible difficulties in extensions of the Yee scheme to non-orthogonal or unstructured grids, discontinuous material parameters, and non-smooth source terms, and also offers potential remedies.

Keywords: Maxwell's equations, explicit time stepping, finite element methods, mass-lumping, Yee-like schemes

AMS subject classifications: 35Q61, 65M60

1. INTRODUCTION

We consider the efficient numerical simulation of electromagnetic wave propagation through linear non-dispersive lossy media. As the basic mathematical model, we use Maxwell's equations in second-order form, i.e.

$$\varepsilon \partial_{tt} E + \sigma \partial_t E + \operatorname{curl}(\nu \operatorname{curl} E) = f, \quad \text{in } \Omega, t > 0, \quad (1)$$

$$n \times (\nu \operatorname{curl} E) = g, \quad \text{on } \partial\Omega, t > 0, \quad (2)$$

Here ε and σ denote the electric permittivity and conductivity, and ν the magnetic reluctivity of the medium; further E is the electric field intensity, f , g describe the excitation by volume or surface currents, and Ω is the computational domain.

One of the standard approaches for solving (1)–(2) numerically is the Yee scheme and its relatives, e.g., the finite difference time domain (FDTD) method and the

E-mail address: bogdan.radu@ricam.oeaw.ac.at, herbert.egger@jku.at.

finite-integration technique (FIT); see [38], [34, 35], and [36, 37] for details. The common algebraic form of all these methods reads

$$\mathbf{M}_\varepsilon \frac{\mathbf{E}^{n+1} - 2\mathbf{E}^n + \mathbf{E}^n}{\tau^2} + \mathbf{M}_\sigma \frac{\mathbf{E}^{n+1} - \mathbf{E}^{n-1}}{2\tau} + \mathbf{K}_\nu \mathbf{E}^n = \mathbf{f}^n + \mathbf{g}^n. \quad (3)$$

This allows for an efficient realization by explicit time stepping, whenever the mass matrices $\mathbf{M}_\varepsilon, \mathbf{M}_\sigma$ are diagonal. On structured orthogonal grids and for homogeneous material distributions, such constructions are possible and lead to second-order accurate approximations in space and time; see e.g. [6, 35, 38]. These results remain valid for non-uniform orthogonal grids [28]; further see [6, 7] for related higher-order methods. The extension of the Yee scheme to discontinuous material parameters or source terms and to non-orthogonal or even unstructured grids is, however, not straightforward; see [17, 20, 32, 33] and [2, 4, 5] for some attempts in the latter case. To the best of our knowledge, a rigorous convergence analysis of Yee-like schemes in such situations is not available up to date.

An alternative approach that allows the construction of stable schemes for structured as well as unstructured grids, and also for discontinuous material parameters, is offered by finite element discretizations. A rigorous error analysis for various methods can be developed; see e.g. [23, 24, 25]; we refer to [6, 18] for an overview of different approaches, their analysis, and further references. Together with the leap-frog time-stepping scheme, the finite element approximation of (1)–(2) again leads to algebraic systems of the form (3). In contrast to the finite difference schemes mentioned above, the mass matrices \mathbf{M}_ε and \mathbf{M}_σ are, however, usually not diagonal, and the realization of (3) thus requires the solution of linear systems in every time step. Therefore, the use of implicit time-stepping schemes has been advocated in the literature [22, 26].

This inherent disadvantage of finite element approximations can be overcome by mass-lumping, which aims at replacing $\mathbf{M}_\varepsilon, \mathbf{M}_\sigma$ in (3) by diagonal or block-diagonal matrices. For orthogonal grids, corresponding schemes have been proposed in [7] and modifications for unstructured grids have been considered in [11, 12]; we also refer to [6] for a detailed discussion. A full convergence analysis for a second order method has been given recently in [10, 31], and in [19] higher order approximations of Maxwell's equations were obtained based on staggered grid complexes. Another approach for generating non-conforming finite element approximations with block-diagonal mass matrices is provided by discontinuous-Galerkin methods [8, 16]. For low-order approximations however, these methods suffer from a substantial increase in the number of degrees of freedom; we refer to [15] for comparison with mass-lumping schemes in the context of elastodynamics.

Main contributions. In this paper, we propose and analyze a fully discrete finite element approximation for (1)–(2) which can be considered as a natural extension of the Yee scheme to unstructured grids. This method involves only one degree of freedom for most edges and it can be realized efficiently as an explicit time-stepping scheme; moreover, a full convergence analysis is possible. The approach and its analysis are based on the following key ideas, already presented in [9]: First, a finite element method is considered involving two degrees of freedom on each edge. Mass lumping is achieved by appropriate numerical quadrature and a corresponding choice of basis functions, and a full error analysis can be developed based on standard

arguments. In a second step, the method is then reduced on the algebraic level to a scheme that involves only one degree of freedom for most edges. While a direct variational characterization of this scheme is no longer possible, its close relation to the first method nevertheless allows to develop a rigorous error analysis. Compared to [9], some non-trivial modifications are required in the construction and the analysis of the proposed methods to deal with non-trivial conductivities σ and inhomogeneous problem data f, g . On orthogonal grids and for special situations, the reduced method becomes equivalent to the traditional Yee scheme. The analysis of this paper therefore also offers some recipes for extensions of the Yee scheme to non-orthogonal grids and discontinuous parameters and problem data. The algebraic form of the numerical scheme obtained after reduction also shares similarities with the approaches of [4, 5], which will be briefly discussed at the end of the manuscript.

Outline. In Section 2, we introduce our notation and basic assumptions. The methods and main results are presented in Section 3. The error analysis is developed in Section 4 and the implementation of the method is discussed in some detail in Section 5. For an illustration of our theoretical results, some computational tests are presented in Section 6, and we close with a short discussion.

2. NOTATION AND BASIC ASSUMPTIONS

We consider a three-dimensional setting and assume that $\Omega \subset \mathbb{R}^3$ is a bounded polyhedral Lipschitz domain. Throughout the paper, we assume that

- (A1) \mathcal{T}_h is a geometrically-conforming non-overlapping partition of Ω into tetrahedral elements $K \in \mathcal{T}_h$; the mesh \mathcal{T}_h is shape-regular and quasi-uniform, i.e., $\gamma h_K^3 \leq |K| \leq h_K^3$ and $\delta h \leq h_K \leq h$ for all $K \in \mathcal{T}_h$ with $\gamma, \delta > 0$.

As usual, h_K and $|K|$ denote the diameter and the volume of the element $K \in \mathcal{T}_h$, and $h = \max_K h_K$ is the global mesh size; see [13] for further details. All results are presented in detail for the three-dimensional setting and unstructured grids, but the translation to two dimensions and structured grids is possible and more or less straightforward; see [31, Chapter 5] and Section 6.

The material parameters and problem data are required to be sufficiently regular and to satisfy the usual physical bounds. Moreover, material discontinuities shall be resolved by the mesh. For ease of presentation, we thus assume that

- (A2) $\varepsilon, \sigma, \nu \in P_0(\mathcal{T}_h)$ and $0 \leq \varepsilon, \sigma, \nu \leq \bar{c}$ and $\varepsilon, \nu \geq \underline{c}$ for some constants $\underline{c}, \bar{c} > 0$.
- (A3) $f : [0, T] \rightarrow L^2(\Omega)^3$ and $g : [0, T] \rightarrow L^2(\partial\Omega)^3$ are smooth functions of time, with $f(0) = 0$ and $g(0) = 0$, and the initial conditions are $E(0) = \partial_t E(0) = 0$.

We write $P_k(\mathcal{T}_h) = \{v : v|_K \in P_k(K), \forall K \in \mathcal{T}_h\}$ for the space of piecewise polynomials of degree k on \mathcal{T}_h . Under these assumptions, the existence of a unique solution to (1)–(2) can be established by standard arguments; see e.g. [21, 23]. Also, more general conditions could be treated with minor modifications to our analysis.

Function spaces. We use standard symbols $L^2(\Omega)$, $H^1(\Omega)$, and $H(\text{curl}; \Omega)$ for the spaces of square-integrable function with square integrable weak gradients and curls, respectively; see [27] for details. The norm of a space X is denoted by $\|\cdot\|_X$ and we

will often write $\langle a, b \rangle = \int_{\Omega} a \cdot b \, dx$ and $\langle a, b \rangle_{\partial} = \int_{\partial\Omega} a \cdot b \, ds(x)$ for the scalar products of two functions in $L^2(\Omega)^3$ and $L^2(\partial\Omega)^3$, respectively. For the error analysis, we use $H^k(\mathcal{T}_h) = \{v \in L^2(\Omega) : v|_K \in H^k(K), \forall K \in \mathcal{T}_h\}$, to denote spaces of piecewise smooth functions, and we write $\|v\|_{H^k(\mathcal{T}_h)} = (\sum_K \|v\|_{H^k(K)}^2)^{1/2}$ for the corresponding norms. We further denote by $L^p(0, T; X)$ the Bochner spaces of functions with values in X whose p -th power is integrable in time. The functions in $W^{k,p}(0, T; X)$ further have weak derivatives in $L^p(0, T; X)$. For brevity, we will sometimes write $L^p(X)$ and $W^{k,p}(X)$, and omit explicit reference to the time interval.

Space discretization. For the spatial approximation of the electric field E , we first consider Nédélec finite elements of type II, i.e.

$$V_h = \{v_h \in H(\text{curl}; \Omega) : v_h|_K \in P_1(K)^3 \, \forall K \in \mathcal{T}_h\}.$$

This amounts to the space of piecewise linear vector-valued functions with tangential continuity across element boundaries; see [1, 27, 29]. Let us recall that functions in V_h have two degrees of freedom for every edge, and the canonical interpolation operator for the space is given by $\Pi_h : H(\text{curl}; \Omega) \cap H^1(\mathcal{T}_h)^3 \rightarrow V_h$, with

$$\int_e \Pi_h v \cdot \tau_e p_e \, ds = \int_e v \cdot \tau_e p_e \, ds \quad \forall p_e \in P_1(e), \, e \in \mathcal{E}_h.$$

Here $\mathcal{E}_h = \{e_{ij} : i < j\}$ is the set of edges $e_{ij} = (v_i, v_j)$ and τ_e is the unit tangential vector on $e = e_{ij}$ pointing from vertex v_i to v_j with $i < j$.

For a given subset $\tilde{\mathcal{E}}_h \subset \mathcal{E}_h$ of edges, we define the corresponding subspace

$$\tilde{V}_h = \{v_h \in V_h : v_h \cdot \tau_e \in P_0(e) \, \forall e \in \tilde{\mathcal{E}}_h\} \subset V_h,$$

which consists of functions in V_h having only constant tangential trace, and therefore only one degree of freedom for edges $e \in \tilde{\mathcal{E}}_h$. We thus call \tilde{V}_h the *reduced space* in the following. The canonical interpolation operator for \tilde{V}_h is given by $\tilde{\Pi}_h : H^1(\mathcal{T}_h)^3 \cap H(\text{curl}; \Omega) \rightarrow \tilde{V}_h$ with

$$\int_e \tilde{\Pi}_h v \cdot \tau_e p_e \, ds = \int_e v \cdot \tau_e p_e \, ds \quad \forall p_e \in P_{k_e}(e), \, e \in \mathcal{E}_h,$$

and with degree $k_e = 0$ for $e \in \tilde{\mathcal{E}}_h$ and $k_e = 1$ for $e \in \mathcal{E}_h \setminus \tilde{\mathcal{E}}_h$. For any choice of $\tilde{\mathcal{E}}_h \subset \mathcal{E}_h$, we have the inclusions

$$\mathcal{N}_0(\mathcal{T}_h) \cap H(\text{curl}; \Omega) \subset \tilde{V}_h \subset \mathcal{NC}_1(\mathcal{T}_h) \cap H(\text{curl}; \Omega).$$

Here \mathcal{N}_0 and \mathcal{NC}_1 denote the lowest order Nédélec elements of type I and II. This ensures good approximation properties for both spaces; see [1, 30, 29] for details. For the choice $\tilde{\mathcal{E}}_h = \mathcal{E}_h$ or $\tilde{\mathcal{E}}_h = \emptyset$, one of the two inclusions becomes an identity.

Mass lumping. For the approximation of some of the integrals arising in the finite element approximation of (1)–(2), we use numerical integration by the vertex rule; this will allow for mass-lumping later on. For ease of notation, we introduce

$$\langle a, b \rangle_h = \sum_T \frac{|T|}{4} \sum_{v_i \in T} a(v_i) \cdot b(v_i).$$

Here a, b are assumed to be piecewise smooth vector-valued functions over the mesh \mathcal{T}_h . Let us note that the quadrature is exact if $a \cdot b \in P_1(\mathcal{T}_h)$.

Time discretization. Let $\tau = T/N$ and $t^n = n\tau$ be a sequence of uniformly spaced time steps. Further let $(a^n)_{n \geq 0} \subset X$ be a sequence in some vector space X . Then

$$\partial_{\tau\tau} a^n := \frac{a^{n+1} - 2a^n + a^{n-1}}{\tau^2} \quad \text{and} \quad \partial_\tau a^{n-1/2} := \frac{a^n - a^{n-1}}{\tau},$$

are used to denote the standard central difference quotients approximating the second and first derivative at time $t = t^n$ and $t = t^{n-1/2} = t^n - \frac{1}{2}\tau$, respectively.

3. MAIN RESULTS

For the numerical approximation of (1)–(2) with homogeneous initial conditions, see assumption (A3), we now consider the following fully discrete scheme.

Method 3.1. Let $\tilde{\mathcal{E}}_h \subset \mathcal{E}_h$ and $\tilde{\Pi}_h : V_h \rightarrow \tilde{V}_h$ denote the appropriate projection. Find $E_h^n \in V_h$, $0 \leq n \leq N$, with $E_h^0 = E_h^1 = 0$ and such that

$$\begin{aligned} \langle (\varepsilon + \frac{\tau}{2}\sigma)\partial_{\tau\tau} E_h^n, v_h \rangle_h + \langle \sigma\tilde{\Pi}_h\partial_\tau E_h^{n-1/2}, \tilde{\Pi}_h v_h \rangle_h + \langle \nu \operatorname{curl} E_h^n, \operatorname{curl} v_h \rangle \\ = \langle f(t^n), v_h \rangle + \langle g(t^n), v_h \rangle_{\partial\Omega}, \quad \forall 1 \leq n < N. \end{aligned} \quad (4)$$

The solution (sequence) will be abbreviated by the symbol $E_h = (E_h^n)_{0 \leq n \leq N}$.

Independently of the choice of the set of edges $\tilde{\mathcal{E}}_h \subset \mathcal{E}_h$, on which the number of degrees of freedom is reduced, the implementation of the method leads to a finite-dimensional recursion of the form

$$\mathbf{M}_{\varepsilon+\tau\sigma/2} \frac{\mathbf{E}^{n+1} - 2\mathbf{E}^n + \mathbf{E}^{n-1}}{\tau^2} + \hat{\mathbf{M}}_\sigma \frac{\mathbf{E}^n - \mathbf{E}^{n-1}}{\tau} + \mathbf{K}_\nu \mathbf{E}^n = \mathbf{f}^n + \mathbf{g}^n. \quad (5)$$

The well-posedness of the discretization scheme then follows immediately from the regularity of the matrix $\mathbf{M}_{\varepsilon+\tau\sigma/2}$, which is a direct consequence of Lemma 4.3 below. In Section 5, we further show that an appropriate choice of basis functions for the space V_h , adopted to the numerical quadrature, leads to a block-diagonal mass matrix $\mathbf{M}_{\varepsilon+\tau\sigma/2}$, such that time stepping in (5) can be realized efficiently.

The algebraic form (5) reveals that Method 3.1 is based on an explicit time-stepping scheme and a restriction on the time step size τ is, therefore, required to ensure discrete stability and convergence with $h, \tau \rightarrow 0$. We thus assume that

(A4) the time step $\tau > 0$ is chosen to satisfy for all $v_h \in V_h$ the inequality

$$\frac{\tau^2}{4} \langle \nu \operatorname{curl} v_h, \operatorname{curl} v_h \rangle + \frac{\tau}{2} \left| \langle \sigma\tilde{\Pi}_h v_h, \tilde{\Pi}_h v_h \rangle - \langle \sigma v_h, v_h \rangle \right| \leq \frac{1}{2} \langle \varepsilon v_h, v_h \rangle_h.$$

For conductivity $\sigma = 0$ and $\langle \cdot, \cdot \rangle_h = \langle \cdot, \cdot \rangle$, this assumption reduces to the usual CFL condition as used, e.g., in [6, 18]. Under our assumptions on the mesh and the model parameters, one can verify that $\tau \leq Ch$ for some appropriate constant $C > 0$ is sufficient to guarantee condition (A4); see Section 6. In practice, an appropriate time step τ satisfying (A4) can be found by performing a few vector iterations.

To guarantee good approximation properties, we further need some restriction on the set $\tilde{\mathcal{E}}_h$ of edges, on which the polynomial order is reduced. We thus require that

(A5) σ is continuous across edges $e \in \tilde{\mathcal{E}}_h$ inside Ω , and $\sigma = 0$ for all $e \in \tilde{\mathcal{E}}_h$ on $\partial\Omega$.

This condition simply means that we stay with two degrees of freedom on edges where the conductivity σ is either discontinuous or non-trivial at the boundary. The reason for this restriction will become clear from the error analysis given in the next section and its necessity will be illustrated by numerical tests.

For ease of notation, we write $\|u_h\|_{\ell_\infty(X)} = \max_{0 \leq k \leq N-1} \|u_h^{n+1/2}\|_X$ in the following statements, and we write $u^{n+1/2} = u(t^{n+1/2})$ for functions u that are continuous in time. We further denote by $\widehat{u}^{n+1/2} = \frac{1}{2}(u^{n+1} + u^n)$ the average at intermediate time steps. This allows us to present our first main result as follows.

Theorem 3.2. *Let E be a sufficiently smooth solution of (1)–(2) and let (A1)–(A5) hold. Then Method 3.1 is well-defined and the discrete solution $E_h = (E_h^n)_n$ satisfies*

$$\|\partial_t E - \partial_\tau E_h\|_{\ell_\infty(L^2(\Omega))} + \|\operatorname{curl}(E - \widehat{E}_h)\|_{\ell_\infty(L^2(\Omega))} \leq C(E)h + C'(E)\tau^2,$$

with constants

$$\begin{aligned} C(E) &= \|\partial_t E\|_{L^\infty(H^1(\mathcal{T}_h))} + \|\operatorname{curl} E\|_{L^\infty(H^1(\mathcal{T}_h))} + \|\partial_{tt} E\|_{L^\infty(H^1(\mathcal{T}_h))} \\ &\quad + \|\operatorname{curl} \partial_t E\|_{L^1(H^1(\mathcal{T}_h))} + \|\partial_t E\|_{L^1(H^1(\Omega))}, \\ C'(E) &= \|\partial_{ttt} E\|_{L^1(L^2(\Omega))} + \|\partial_{tt} E\|_{L^1(L^2(\Omega))} + \|\operatorname{curl} \partial_{tt} E\|_{L^1(H^1(\mathcal{T}_h))}. \end{aligned}$$

The implementation leads to a time-stepping scheme (5), and for an appropriate choice of a basis, the matrix $\mathbf{M}_{\varepsilon+\tau\sigma/2}$ is block-diagonal, while $\widehat{\mathbf{M}}_\sigma$ and \mathbf{K}_ν are sparse.

The convergence results is proven in Section 4, while the algebraic structure of the scheme is derived in Section 5. Let us note that the assertions hold, in particular, for the choice $\widetilde{\mathcal{E}}_h = \emptyset$, for which the projection $\widetilde{\Pi}_h$ drops out and the method as well as its implementation become somewhat simpler; see [31] for details.

The Yee-like scheme. The reason for introducing the projection $\widetilde{\Pi}_h$ in Method 3.1 lies in the following important observation, which is summarized as our second main result and leads to the reduced Yee-like scheme announced in the introduction.

Theorem 3.3. *Let the assumptions of Theorem 3.2 be valid and $E_h = (E_h^n)_n$ denote the solution of Method 3.1. Further define $\widetilde{E}_h^n = \widetilde{\Pi}_h E_h^n$ for all $n \geq 0$. Then*

$$\|\partial_t E - \partial_\tau \widetilde{E}_h\|_{\ell_\infty(L^2(\Omega))} + \|\operatorname{curl}(E - \widehat{\widetilde{E}}_h)\|_{\ell_\infty(L^2(\Omega))} \leq C(E)h + C'(E)\tau^2,$$

with constants $C(E)$ and $C'(E)$ of the same form as in Theorem 3.2. Moreover, the coefficients of the solution \widetilde{E}_h can be computed by the time-stepping scheme

$$\partial_{\tau\tau} \widetilde{E}^n = \widetilde{\mathbf{M}}_{\varepsilon+\tau\sigma/2}^{-1} (-\widetilde{\mathbf{M}}_\sigma \partial_\tau \widetilde{E}^{n-1/2} - \widetilde{\mathbf{K}}_\nu \widetilde{E}^n) + \widetilde{\mathbf{F}}^n + \widetilde{\mathbf{G}}^n, \quad (6)$$

and for an appropriate choice of basis for \widetilde{V}_h , the matrices $\widetilde{\mathbf{M}}_{\varepsilon+\tau\sigma/2}^{-1}$, $\widetilde{\mathbf{M}}_\sigma$ and $\widetilde{\mathbf{K}}_\nu$ are sparse and the vectors $\widetilde{\mathbf{F}}^n$ and $\widetilde{\mathbf{G}}^n$ can be cheaply assembled from \mathbf{f}^n and \mathbf{g}^n in (5).

Remark 3.4. If $\sigma = 0$, we may choose $\widetilde{\mathcal{E}}_h = \mathcal{E}_h$ and obtain an explicit time-stepping method for Maxwell's equations with exactly one degree of freedom per edge. For orthogonal grids and homogeneous data $f, g \equiv 0$, the presented approach becomes equivalent to the Yee scheme; see [9] for details.

The two assertions of Theorem 3.3 are again proven in the following two sections.

Remark 3.5. Let us emphasize that the matrix $\tilde{\mathbf{M}}_{\varepsilon+\tau\sigma/2}$ in (6) has a sparse inverse, but it is not a sparse matrix by itself. In contrast to (5), which corresponds to Method 3.1, we can not give a variational characterization of the scheme (6) in closed form. This poses a severe challenge for the analysis of this method which can be overcome only by a somewhat non-standard analysis.

4. PROOF OF CONVERGENCE RATES

In this section, we establish the convergence rates stated in Theorem 3.2 and 3.3. To be able to do so, we require a couple of auxiliary results, which are stated first.

4.1. Projection operators. For later reference, we collect some well-known properties of projection operators arising in our error analysis below.

Lemma 4.1. *Let (A1) hold, $\tilde{\mathcal{E}}_h \subset \mathcal{E}_h$, and $\Pi_h, \tilde{\Pi}_h$ be defined as in Section 2. Then*

$$\begin{aligned} \|E - \tilde{\Pi}_h E\|_{L^2(K)} &\leq Ch \|E\|_{H^1(K)}, \\ \|\operatorname{curl}(E - \tilde{\Pi}_h E)\|_{L^2(K)} &\leq Ch \|\operatorname{curl} E\|_{H^1(K)}, \end{aligned}$$

for all $E \in H^1(\mathcal{T}_h)$ and $K \in \mathcal{T}_h$ with a constant C depending only on γ, δ in assumption (A1). The same estimates also hold for the projection operator Π_h .

The proof of the assertions follows from the arguments given in [1, Sec. 2.5]. In our analysis, we will also make use of the L^2 -orthogonal projection $\pi_\omega^0 : L^2(\omega) \rightarrow P_0(\omega)$ to constants for certain subsets $\omega \subset \Omega$, which is defined by

$$\int_\omega \pi_\omega^0 v \, dx = \int_\omega v \, dx.$$

The same symbol will also be used for the projection of vector-valued functions.

Lemma 4.2. *Let (A1) hold and $\omega = K$ for $K \in \mathcal{T}_h$ or $\omega = \bigcup_{K \cap e=e} K$ for $e \in \mathcal{E}_h$. Then the projection error can be estimated by*

$$\|v - \pi_\omega^0 v\|_{L^2(\omega)} \leq Ch \|v\|_{H^1(\omega)}$$

for all $v \in H^1(\omega)$ with constant C depending only on γ, δ in assumption (A1).

The proof of this assertion is based on the Poincaré–Friedrichs inequality [14, Thm. 1.1] and standard scaling arguments; also see [3, Ch. 4]. Here we use that the sets ω appearing in the lemma are uniformly star-shaped with respect to balls of size h , which follows from assumption (A1) on the mesh, and hence C is universal.

We will further write $\pi_h^0 : L^2(\Omega) \rightarrow P_0(\mathcal{T}_h)$ for the projection to piecewise constants over the mesh \mathcal{T}_h , defined by $(\pi_h^0 v)|_K = \pi_K^0(v|_K)$, and note that

$$\|v - \pi_h^0 v\|_{L^2(K)} \leq Ch \|v\|_{H^1(K)},$$

which follows immediately from the assertion of the previous lemma.

4.2. Properties of the quadrature rule. As a second ingredient, we now state some elementary facts about the quadrature rule introduced in Section 2.

Lemma 4.3. *Let (A1) hold and $\alpha \in P_0(\mathcal{T}_h)$ with $\alpha \geq 0$. Then*

$$c \langle \alpha v_h, v_h \rangle \leq \langle \alpha v_h, v_h \rangle_h \leq C \langle \alpha v_h, v_h \rangle \quad \forall v_h \in V_h,$$

with uniform constants $c, C > 0$ depending only on the bounds in assumption (A1).

Proof. We consider a single element $K \in \mathcal{T}_h$ and abbreviate $\langle a, b \rangle_K = \int_K a \cdot b \, dx$ and $\langle a, b \rangle_{h,K} = \frac{|K|}{4} \sum_i a(v_i) \cdot b(v_i)$. By mapping to the reference element, using the finite dimensionality of $P_1(K)$ ³, and noting that $\alpha \geq 0$ is piecewise constant, we get

$$c \langle \alpha v_h, v_h \rangle_K \leq \langle \alpha v_h, v_h \rangle_{h,K} \leq C \langle \alpha v_h, v_h \rangle_K,$$

with constants c, C that only depend on the shape regularity of the element K . The assertion of the lemma then follows by summation over all elements $K \in \mathcal{T}_h$. \square

As a direct consequence of the previous result, we obtain the following assertions:

Corollary 4.4. *Let (A1) hold. Then $\|v_h\|_h^2 = \langle v_h, v_h \rangle_h$ defines a norm on V_h and*

$$c_1 \|v_h\|_{L^2(\Omega)} \leq \|v_h\|_h \leq c_2 \|v_h\|_{L^2(\Omega)} \quad \forall v_h \in V_h.$$

Further let $\alpha \in P_0(\mathcal{T}_h)$ with $0 < \underline{\alpha} \leq \alpha \leq \bar{\alpha}$. Then $\langle \alpha u_h, v_h \rangle_h$ defines a continuous and elliptic symmetric bilinear form on V_h , more precisely

$$c_1 \underline{\alpha} \|u_h\|_{L^2(\Omega)}^2 \leq \langle \alpha u_h, u_h \rangle_h \quad \text{and} \quad \langle \alpha u_h, v_h \rangle_h \leq c_2 \bar{\alpha} \|u_h\|_{L^2(\Omega)} \|v_h\|_h \quad \forall u_h, v_h \in V_h.$$

These properties immediately imply the well-posedness of Method 3.1. As a next ingredient for our analysis, we analyze the quadrature error.

Lemma 4.5. *Let assumption (A1) hold and let*

$$\delta_h(\alpha u_h, v_h) := \langle \alpha u_h, v_h \rangle_h - \langle \alpha u_h, v_h \rangle$$

denote the quadrature error for some $\alpha \in P_0(\mathcal{T}_h)$. Then

$$|\delta_h(\alpha \tilde{\Pi}_h u, v_h)| \leq Ch \|u\|_{H^1(\mathcal{T}_h)} \|v_h\|_{L^2(\Omega)} \quad \forall u \in H^1(\mathcal{T}_h)^3, v_h \in V_h,$$

with constant C depending only on $\|\alpha\|_{L^\infty(\Omega)}$ and the constants in assumption (A1).

Proof. We define the local error $\delta_{h,K}(\alpha u_h, v_h) := \langle \alpha u_h, v_h \rangle_{h,K} - \langle \alpha u_h, v_h \rangle_K$, and split

$$|\delta_{h,K}(\alpha \tilde{\Pi}_h u, v_h)| \leq |\alpha \delta_{h,K}(\pi_h^0 u, v_h)| + |\alpha \delta_K(\tilde{\Pi}_h u - \pi_h^0 u, v_h)| = (i) + (ii),$$

where we used that α is piecewise constant. Since the quadrature rule integrates linear polynomials exactly, we obtain (i) = 0. The second term can again be bounded elementwise. We may therefore omit α and obtain

$$\begin{aligned} |\delta_K(\tilde{\Pi}_h u - \pi_h^0 u, v_h)| &\leq (1 + c_1) \|\tilde{\Pi}_h u - \pi_h^0 u\|_{L^2(K)} \|v_h\|_{L^2(K)} \\ &\leq C (\|u - \pi_h^0 u\|_{L^2(K)} + \|u - \tilde{\Pi}_h u\|_{L^2(K)}) \|v_h\|_{L^2(K)} \\ &\leq C' h \|u\|_{H^1(K)} \|v_h\|_{L^2(K)}. \end{aligned}$$

Here we used the assertions of Corollary 4.4 and the Cauchy-Schwarz inequality in the first step, and the projection error estimates of Lemma 4.1 and 4.2 in the last. Scaling by the constant α and summation over all elements leads to the assertion. \square

4.3. Estimates for the loss term. We now present a particular approximation property, which explains why the degree of approximation can be reduced on the edges in the set $\tilde{\mathcal{E}}_h$ satisfying assumption (A5) without decreasing the accuracy.

Lemma 4.6. *Let $\lambda_i \in P_1(\mathcal{T}_h) \cap H^1(\Omega)$ denote the barycentric coordinates defined by $\lambda_i(v_j) = \delta_{ij}$ for all vertices v_j of the mesh. To every edge $e_{ij} \in \mathcal{E}_h$, we define*

$$\Phi_{ij} = \lambda_i \nabla \lambda_j \quad \text{and} \quad \Phi_{ji} = -\lambda_j \nabla \lambda_i. \quad (7)$$

These basis functions are linearly independent and $V_h = \text{span}\{\Phi_{ij}, \Phi_{ji} : e_{ij} \in \mathcal{E}_h\}$. Hence the functions defined in (7) comprise a basis for V_h .

The assertion follows immediately from the considerations in [1, 29]. In the subsequent analysis, we will also make use of the following norm equivalence.

Lemma 4.7. *Let (A1) hold and let $v_h \in V_h$, i.e., $v_h = \sum_{e_{ij} \in \mathcal{E}_h} \mathbf{v}_{ij} \Phi_{ij} + \mathbf{v}_{ji} \Phi_{ji}$ for appropriate coefficients $\mathbf{v}_{ij}, \mathbf{v}_{ji} \in \mathbb{R}$. Further let $\omega(e_{ij}) = \bigcup_{K \cap e_{ij} = e_{ij}} K$ denote the patch of elements containing the edge e_{ij} . Then*

$$\| \|v_h\| \|_h^2 := \sum_{e_{ij} \in \mathcal{E}_h} \mathbf{v}_{ij}^2 \|\Phi_{ij}\|_{L^2(\omega(e_{ij}))}^2 + \mathbf{v}_{ji}^2 \|\Phi_{ji}\|_{L^2(\omega(e_{ij}))}^2$$

defines a norm on V_h which is equivalent to $\|\cdot\|_{L^2(\Omega)}$. More precisely, one has

$$c'_1 \|v_h\|_{L^2(\Omega)} \leq \| \|v_h\| \|_h \leq c'_2 \|v_h\|_{L^2(\Omega)} \quad \forall v_h \in V_h$$

with uniform constants $c'_1, c'_2 > 0$ depending only on the bounds in assumption (A1).

The result again follows by scaling arguments and the equivalence of norms on finite-dimensional spaces. Using these observations, we can now prove the following.

Lemma 4.8. *Let (A1)–(A2) and (A5) hold. Then for any $u \in H^1(\Omega)^3$, we have*

$$\langle \sigma \tilde{\Pi}_h u, \tilde{\Pi}_h v_h - v_h \rangle \leq C h \|u\|_{H^1(\Omega)} \|v_h\|_{L^2(\Omega)} \quad \forall v_h \in V_h,$$

with a uniform constant C depending only on the bounds in the assumptions.

Proof. We start by considering a special test function $v_h = \Phi_{ij}$, where Φ_{ij} is one of the basis functions introduced in Lemma 4.6. We then split

$$\begin{aligned} \langle \sigma \tilde{\Pi}_h u, \tilde{\Pi}_h \Phi_{ij} - \Phi_{ij} \rangle &= \langle \sigma \pi_\omega^0 u, \tilde{\Pi}_h \Phi_{ij} - \Phi_{ij} \rangle + \langle \sigma (\tilde{\Pi}_h u - \pi_\omega^0 u), \tilde{\Pi}_h \Phi_{ij} - \Phi_{ij} \rangle \\ &= (i) + (ii), \end{aligned}$$

where $\pi_\omega^0 : L^2(\omega) \rightarrow P_0(\omega)$ is the L^2 -projection onto constants on the support $\omega = \omega(e_{ij})$ of the basis function Φ_{ij} . If $e_{ij} \in \mathcal{E}_h \setminus \tilde{\mathcal{E}}_h$, we have $\Phi_{ij} = \tilde{\Pi}_h \Phi_{ij}$, which means that (i) = 0 in this case. If $e_{ij} \in \tilde{\mathcal{E}}_h$, on the other hand, then we deduce from assumptions (A2) and (A5) that σ is constant on the patch $\omega = \omega(e_{ij})$. We can thus find a vector $b_1 \in P_1(\omega)^3$ such that $\text{curl } b_1 = \sigma \pi_\omega^0 u$, and evaluate

$$\begin{aligned} (i) &= \langle \text{curl } b_1, \tilde{\Pi}_h \Phi_{ij} - \Phi_{ij} \rangle_\omega \\ &= \langle b_1, \text{curl}(\tilde{\Pi}_h \Phi_{ij} - \Phi_{ij}) \rangle_\omega + \langle b_1, n \times (\tilde{\Pi}_h \Phi_{ij} - \Phi_{ij}) \rangle_{\partial\omega} = (iii) + (iv). \end{aligned}$$

By elementary computations, see Lemma 5.1 below, one can verify that

$$\tilde{\Pi}_h \Phi_{ij} - \Phi_{ij} = \nabla(\lambda_i \lambda_j), \quad \text{and hence } \text{curl}(\tilde{\Pi}_h \Phi_{ij} - \Phi_{ij}) = 0, \quad (8)$$

which in turn implies (iii) = 0. By definition of the basis functions, the tangential components of Φ_{ij} and also that of $\tilde{\Pi}_h \Phi_{ij}$ vanish on $\partial\omega(e_{ij})$, unless e_{ij} is a boundary

edge, which is excluded by assumption (A5). Hence $(iv) = 0$, and as a consequence, we see that $(i) = 0$. Since we assumed $u \in H^1(\Omega)$, we may further bound

$$(ii) \leq Ch \|u\|_{H^1(\omega)} \|\Phi_{ij}\|_{L^2(\omega)}$$

by employing the estimates of Lemma 4.1 and 4.2. In summary, we thus have

$$\langle \sigma \tilde{\Pi}_h u, \tilde{\Pi}_h \Phi_{ij} - \Phi_{ij} \rangle \leq Ch \|u\|_{H^1(\omega)} \|\Phi_{ij}\|_{L^2(\omega)}.$$

The same estimate is obtained for the basis functions Φ_{ji} . By Lemma 4.6, any test function in V_h can be expanded as $v_h = \sum_{e_{ij}} \mathbf{v}_{ij} \Phi_{ij} + \mathbf{v}_{ji} \Phi_{ji}$, and by splitting and summing over all elements, we immediately obtain

$$\begin{aligned} \langle \sigma \tilde{\Pi}_h u, \tilde{\Pi}_h v_h - v_h \rangle &\leq Ch \sum_{e_{ij}} \|u\|_{H^1(\omega(e_{ij}))} (\mathbf{v}_{ij} \|\Phi_{ij}\|_{L^2(\omega(e_{ij}))} + \mathbf{v}_{ji} \|\Phi_{ji}\|_{L^2(\omega(e_{ij}))}) \\ &\leq Ch \left(\sum_{e_{ij}} \|u\|_{H^1(\omega(e_{ij}))}^2 \right)^{1/2} \|v_h\|_h \leq c'' h \|u\|_{H^1(\Omega)} \|v_h\|_{L^2(\Omega)}. \end{aligned}$$

Here we used the Cauchy-Schwarz inequality in the second step, the finite overlap of the patches, and the norm equivalence of Corollary 4.4 in the last. \square

4.4. Discrete stability. We now derive discrete stability estimates for solutions of Method 3.1. To simplify the presentation, we introduce the short-hand notation

$$\|v_h\|_\alpha^2 := \langle \alpha v_h, v_h \rangle, \quad \|v_h\|_{h,\alpha}^2 := \langle \alpha v_h, v_h \rangle_h,$$

for non-negative piecewise constant parameters $\alpha \in P_0(\mathcal{T}_h)$. Furthermore, we use

$$\hat{u}_h^{n+1/2} = \frac{1}{2}(u_h^n + u_h^{n+1}) \quad \text{and} \quad \partial_\tau \hat{u}_h^n = \frac{1}{2\tau}(u_h^{n+1} - u_h^{n-1}).$$

As a final ingredient, we introduce a discrete energy functional, defined by

$$\begin{aligned} \mathcal{E}_h(u_h^n, u_h^{n+1}) &:= \|\partial_\tau u_h^{n+1/2}\|_{h,\varepsilon}^2 + \|\operatorname{curl} \hat{u}_h^{n+1/2}\|_\nu^2 \\ &\quad - \frac{\tau^2}{4} \|\operatorname{curl} \partial_\tau u_h^{n+1/2}\|_\nu^2 - \frac{\tau}{2} \left(\|\tilde{\Pi}_h \partial_\tau u_h^{n+1/2}\|_{h,\sigma}^2 - \|\partial_\tau u_h^{n+1/2}\|_{h,\sigma}^2 \right). \end{aligned}$$

We begin with some elementary auxiliary observations.

Lemma 4.9. *Let (A1)–(A2) and (A4) hold and $u_h^n, u_h^{n+1} \in V_h$ be given. Then*

$$\frac{2}{3} \mathcal{E}_h(u_h^n, u_h^{n+1}) \leq \|\partial_\tau u_h^{n+1/2}\|_{h,\varepsilon}^2 + \|\operatorname{curl} \hat{u}_h^{n+1/2}\|_\nu^2 \leq 2 \mathcal{E}_h(u_h^n, u_h^{n+1}). \quad (9)$$

Proof. The result follows directly from the definition of the energy functional and the CFL condition (A4), which was specifically tailored to obtain this result. \square

We can now establish the required stability estimate for solutions of Method 3.1.

Lemma 4.10 (Discrete stability).

Let (A1)–(A2) and (A4) hold. Further let $\xi_h^n, r_h^n \in V_h$, $n \geq 0$ be given such that

$$\langle (\varepsilon + \frac{\tau}{2}\sigma) \partial_{\tau\tau} \xi_h^n, v_h \rangle_h + \langle \sigma \tilde{\Pi}_h \partial_\tau \xi_h^{n-1/2}, \tilde{\Pi}_h v_h \rangle_h + \langle \nu \operatorname{curl} \xi_h^n, \operatorname{curl} v_h \rangle = \langle r_h^n, v_h \rangle, \quad (10)$$

for all $v_h \in V_h$ and $n \geq 0$. Then for all time steps $0 \leq n < N$, there holds

$$\mathcal{E}_h(\xi_h^n, \xi_h^{n+1}) \leq \mathcal{E}_h(\xi_h^0, \xi_h^1) + 2 \sum_{k=1}^n \tau (r_h^k, \partial_\tau \hat{\xi}_h^k).$$

Proof. We begin by setting $v_h = \partial_\tau \widehat{\xi}_h^n := \frac{1}{2\tau}(\xi_h^{n+1} - \xi_h^{n-1})$ in the identity (10). For the first term on the left-hand side, this results in

$$(\varepsilon \partial_{\tau\tau} \xi_h^n, \partial_\tau \widehat{\xi}_h^n)_h = \frac{1}{2\tau} (\|\partial_\tau \xi_h^{n+1/2}\|_{h,\varepsilon}^2 - \|\partial_\tau \xi_h^{n-1/2}\|_{h,\varepsilon}^2). \quad (11)$$

For the third term in (10), we see in a similar manner that

$$\begin{aligned} (\nu \operatorname{curl} \xi_h^n, \operatorname{curl} \partial_\tau \widehat{\xi}_h^n) &= \frac{1}{2\tau} \left(\|\operatorname{curl} \widehat{\xi}_h^{n+1/2}\|_\nu^2 - \|\operatorname{curl} \widehat{\xi}_h^{n-1/2}\|_\nu^2 \right. \\ &\quad \left. - \frac{\tau^2}{4} \|\operatorname{curl} \partial_\tau \xi_h^{n+1/2}\|_\nu^2 + \frac{\tau^2}{4} \|\operatorname{curl} \partial_\tau \xi_h^{n-1/2}\|_\nu^2 \right). \end{aligned}$$

The loss terms involving σ have to be treated more carefully. Here we use that

$$\begin{aligned} &\langle \frac{\tau}{2} \sigma \partial_{\tau\tau} \xi_h^n, \partial_\tau \widehat{\xi}_h^n \rangle_h + \langle \sigma \widetilde{\Pi}_h \partial_\tau \xi_h^{n-1/2}, \widetilde{\Pi}_h \partial_\tau \widehat{\xi}_h^n \rangle_h \quad (12) \\ &= \langle \frac{\tau}{2} \sigma \partial_{\tau\tau} \xi_h^n, \partial_\tau \widehat{\xi}_h^n \rangle_h - \langle \frac{\tau}{2} \sigma \partial_{\tau\tau} \widetilde{\Pi}_h \xi_h^n, \widetilde{\Pi}_h \partial_\tau \widehat{\xi}_h^n \rangle_h + \langle \sigma \widetilde{\Pi}_h \partial_\tau \widehat{\xi}_h^n, \widetilde{\Pi}_h \partial_\tau \widehat{\xi}_h^n \rangle_h \\ &= \frac{\tau}{2} \frac{1}{2\tau} \left(\|\partial_\tau \xi_h^{n+1/2}\|_{h,\sigma}^2 - \|\partial_\tau \xi_h^{n-1/2}\|_{h,\sigma}^2 \right. \\ &\quad \left. - \|\widetilde{\Pi}_h \partial_\tau \xi_h^{n+1/2}\|_{h,\sigma}^2 + \|\widetilde{\Pi}_h \partial_\tau \xi_h^{n-1/2}\|_{h,\sigma}^2 \right) + \|\widetilde{\Pi}_h \partial_\tau \widehat{\xi}_h^n\|_{h,\sigma}^2. \end{aligned}$$

By summing up the identities (11)–(12), we can deduce that

$$\mathcal{E}_h(\xi_h^n, \xi_h^{n+1}) \leq \mathcal{E}_h(\xi_h^n, \xi_h^{n+1}) + 2\tau \|\widetilde{\Pi}_h \partial_\tau \widehat{\xi}_h^n\|_\sigma^2 = \mathcal{E}_h(\xi_h^{n-1}, \xi_h^n) + 2\tau \langle r_h^n, \partial_\tau \widehat{\xi}_h^n \rangle.$$

The assertion of the theorem then follows by induction over n . \square

4.5. Error estimates. Let us start with proving the estimate of Theorem 3.2. Following standard practice, we split

$$E(t^n) - E_h^n = -(\widetilde{\Pi}_h E(t^n) - E(t^n)) + (\widetilde{\Pi}_h E(t^n) - E_h^n) =: -\eta^n + \xi_h^n,$$

into an interpolation error η^n and a discrete error component ξ_h^n . The use of the particular projection $\widetilde{\Pi}_h$ in this splitting will become important below. With the interpolation error estimates of Lemma 4.1, we immediately obtain

$$\begin{aligned} &\max_{0 \leq n < N} \left(\|\partial_\tau \eta^{n+1/2}\|_{L^2}^2 + \|\operatorname{curl} \widehat{\eta}^{n+1/2}\|_{L^2}^2 \right) \\ &\leq Ch \left(\|\partial_t E\|_{L^\infty(H^1(\mathcal{T}_h))} + \|\operatorname{curl} E\|_{L^\infty(H^1(\mathcal{T}_h))} \right). \end{aligned}$$

For estimating the discrete error ξ_h^n , we first note that $\xi_h^0 = 0$. Moreover, $E_h^1 = 0$ by assumption, and by Taylor expansion, we further see that

$$E(\tau) = E(0) + \tau \partial_t E(0) + \frac{\tau^2}{2} \partial_{tt} E(0) + \frac{\tau^3}{6} \partial_{ttt} E(s_3),$$

for some $0 < s_3 < \tau$. From assumption (A3) and using equation (1), one can see that $E(0) = \partial_t E(0) = \partial_{tt} E(0) = 0$, and hence $\xi_h^1 = \frac{\tau^3}{6} \widetilde{\Pi}_h \partial_{ttt} E(s_3)$. Alternatively, we could also get $\xi_h^1 = \frac{\tau^2}{2} \widetilde{\Pi}_h \partial_{tt} E(s_2)$ for some $0 < s_2 < \tau$ by truncating the Taylor series earlier. In summary, this yields

$$\begin{aligned} \frac{2}{3} \mathcal{E}_h(\xi_h^0, \xi_h^1) &\leq \|\partial_\tau \xi_h^{1/2}\|_{L^2}^2 + \|\operatorname{curl} \widehat{\xi}_h^{1/2}\|_{L^2}^2 = \frac{1}{\tau^2} \|\xi_h^1\|_{L^2}^2 + \frac{1}{4} \|\operatorname{curl} \xi_h^1\|_{L^2}^2 \\ &\leq C\tau^4 \left(\|\partial_{ttt} E\|_{L^\infty(H^1(\mathcal{T}_h))}^2 + \|\partial_{tt} E\|_{L^\infty(H^1(\mathcal{T}_h))}^2 \right). \end{aligned} \quad (13)$$

For the last step, we used the formulas for ξ_h^0 and ξ_h^1 derived above, and the stability estimates $\|\widetilde{\Pi}_h v\|_{L^2} \leq C\|v\|_{H^1}$ and $\|\operatorname{curl} \widetilde{\Pi}_h v\|_{L^2} \leq C\|v\|_{H^1}$ for the projection.

As a next step, let us observe that the continuous solution $E(t)$ of (1)–(2) satisfies $\langle \varepsilon \partial_{tt} E(t^n), v_h \rangle + \langle \sigma \partial_t E(t^n), v_h \rangle + \langle \nu \operatorname{curl} E(t^n), \operatorname{curl} v_h \rangle = \langle f(t^n), v_h \rangle + \langle g(t^n), v_h \rangle_{\partial\Omega}$ for all $v_h \in V_h$ and $n > 0$. By combination with (4), one can then see that the discrete error $\xi_h^n = \tilde{\Pi}_h E(t^n) - E_h^n$ thus satisfies the error equation (10) with

$$\langle r_h^n, v_h \rangle = \langle r_{h,t}^n, v_h \rangle + \langle r_{h,s}^n, v_h \rangle + \langle r_{h,q}^n, v_h \rangle + \langle r_{h,p}^n, v_h \rangle,$$

where the four partial residuals are defined by

$$\begin{aligned} \langle r_{h,t}^n, v_h \rangle &= \langle \varepsilon (\partial_{\tau\tau} E^n - \partial_{tt} E^n), v_h \rangle + \langle \sigma (\partial_\tau \widehat{E}^n - \partial_t E^n), v_h \rangle, \\ \langle r_{h,s}^n, v_h \rangle &= \langle \varepsilon \partial_{tt} \eta^n, v_h \rangle + \langle \sigma \partial_t \eta^n, v_h \rangle + \langle \nu \operatorname{curl} \eta^n, \operatorname{curl} v_h \rangle, \\ \langle r_{h,q}^n, v_h \rangle &= \delta_h \left((\varepsilon + \frac{\tau}{2} \sigma) \tilde{\Pi}_h \partial_{\tau\tau} E^n, v_h \right) + \delta_h \left(\sigma \tilde{\Pi}_h \partial_\tau E^{n-1/2}, v_h \right), \\ \langle r_{h,p}^n, v_h \rangle &= \langle \tilde{\Pi}_h \sigma \partial_\tau E^{n-1/2}, \tilde{\Pi}_h v_h - v_h \rangle, \end{aligned}$$

which represent the temporal, spatial, quadrature, and projection errors, respectively. In the third term, we again used $\delta_h(\alpha u_h, v_h) = \langle \alpha u_h, v_h \rangle_h - \langle \alpha u_h, v_h \rangle$ to abbreviate the quadrature error. We now estimate the four residuals independently.

First residual. By summation over the time steps, we get

$$\begin{aligned} \sum_k \tau \langle r_{h,t}^k, \partial_\tau \widehat{\xi}_h^k \rangle &= \sum_k \tau \langle \varepsilon (\partial_{\tau\tau} E^k - \partial_{tt} E^k), \partial_\tau \widehat{\xi}_h^k \rangle \\ &\quad + \sum_k \tau \langle \sigma (\partial_\tau \widehat{E}^k - \partial_t E^k), \partial_\tau \widehat{\xi}_h^k \rangle = (i) + (ii). \end{aligned}$$

The first term in this expansion can be estimated by Taylor expansion, giving

$$\begin{aligned} |(i)| &\leq \sum_k c\tau^2 \|\partial_{ttt} E\|_{L^1(t^{k-1}, t^k; L^2)} \|\partial_\tau \widehat{\xi}_h^k\|_{L^2} \\ &\leq C\tau^4 \|\partial_{ttt} E\|_{L^1(L^2)}^2 + \frac{1}{56} \|\partial_\tau \xi_h\|_{\ell^\infty(L^2)}^2 \\ &\leq C\tau^4 \|\partial_{ttt} E\|_{L^1(L^2)}^2 + \frac{1}{28} \max_{0 \leq k < N} \mathcal{E}_h(\xi_h^k, \xi_h^{k+1}). \end{aligned}$$

With similar arguments, the second term can be bounded by

$$|(ii)| \leq C\tau^4 \|\partial_{ttt} E\|_{L^1(L^2)}^2 + \frac{1}{28} \max_{0 \leq k < N} \mathcal{E}_h(\xi_h^k, \xi_h^{k+1})$$

Second residual. For the spatial errors, we use

$$\begin{aligned} \sum_k \tau \langle r_{h,s}^k, \partial_\tau \widehat{\xi}_h^k \rangle &= \sum_k \tau \langle \varepsilon \partial_{tt} \eta^k, \partial_\tau \widehat{\xi}_h^k \rangle + \sum_k \tau \langle \sigma \partial_t \eta^k, \partial_\tau \widehat{\xi}_h^k \rangle \\ &\quad + \sum_k \tau \langle \nu \operatorname{curl} \eta^k, \operatorname{curl} \partial_\tau \widehat{\xi}_h^k \rangle = (iii) + (iv) + (v). \end{aligned}$$

By the interpolation error estimates of Lemma 4.1 and Young's inequality, we obtain

$$|(iii) + (iv)| \leq Ch^2 (\|\partial_t E\|_{L^\infty(H^1(\mathcal{T}_h))}^2 + \|\partial_{tt} E\|_{L^\infty(H^1(\mathcal{T}_h))}^2) + \frac{1}{28} \max_{0 \leq k < N} \mathcal{E}_h(\xi_h^k, \xi_h^{k+1}).$$

The factor $\frac{1}{28}$ in the last term was simply chosen small enough for later on. For the remaining term in the second residual, we use summation by parts to arrive at

$$\begin{aligned} |(v)| &\leq \langle \operatorname{curl} \eta^n, \operatorname{curl} \widehat{\xi}_h^{n+1/2} \rangle - \langle \operatorname{curl} \eta^1, \operatorname{curl} \widehat{\xi}_h^{1/2} \rangle \\ &\quad - \sum_k \langle \nu \operatorname{curl} \partial_\tau \eta^{k-1/2}, \operatorname{curl} \widehat{\xi}_h^{k-1/2} \rangle = (vi) + (vii) + (viii). \end{aligned}$$

By the interpolation error estimates and Young's inequality, we obtain

$$\begin{aligned} |(vi) + (vii)| &\leq Ch^2 \|\operatorname{curl} E\|_{L^\infty(H^1(\mathcal{T}_h))}^2 + \frac{1}{56} \|\operatorname{curl} \widehat{\xi}_h\|_{\ell_\infty(L^2)}^2 \\ &\leq Ch^2 \|\operatorname{curl} E\|_{L^\infty(H^1(\mathcal{T}_h))}^2 + \frac{1}{28} \max_{0 \leq k < N} \mathcal{E}_h(\xi_h^k, \xi_h^{k+1}). \end{aligned}$$

By Taylor expansion and arguments similar to before, we further obtain

$$|(viii)| \leq Ch^2 \|\operatorname{curl} \partial_t E\|_{L^1(H^1(\mathcal{T}_h))}^2 + \frac{1}{28} \max_{0 \leq k < N} \mathcal{E}_h(\xi_h^k, \xi_h^{k+1}).$$

The prefactors in these estimates were again simply chosen sufficiently small.

Third residual. Using Lemma 4.5 and Taylor expansion in time, we can estimate the residuals caused by the quadrature errors via

$$\begin{aligned} \sum_k \tau \langle r_{h,q}^k, \partial_\tau \widehat{\xi}_h^k \rangle &\leq Ch^2 (\|\partial_{tt} E\|_{L^1(H^1(\mathcal{T}_h))}^2 + \|\partial_t E\|_{L^1(H^1(\mathcal{T}_h))}^2) + \frac{1}{56} \|\partial_\tau \xi_h\|_{\ell_\infty(L^2)}^2 \\ &\leq Ch^2 (\|\partial_{tt} E\|_{L^1(H^1(\mathcal{T}_h))}^2 + \|\partial_t E\|_{L^1(H^1(\mathcal{T}_h))}^2) + \frac{1}{28} \max_{0 \leq k < N} \mathcal{E}_h(\xi_h^k, \xi_h^{k+1}). \end{aligned}$$

Fourth residual. For the projection errors, we again use Lemma 4.8 and obtain

$$\begin{aligned} \sum_k \tau \langle r_{h,p}^k, \partial_\tau \widehat{\xi}_h^k \rangle &= \sum_k \tau \langle \sigma \widetilde{\Pi}_h \partial_\tau E^{k-1/2}, \widetilde{\Pi}_h \partial_\tau \widehat{\xi}_h^k - \partial_\tau \widehat{\xi}_h^k \rangle \\ &\leq Ch^2 \|\partial_t E\|_{L^1(H^1)}^2 + \frac{1}{56} \|\partial_\tau \xi_h\|_{\ell_\infty(L^2)}^2 \\ &\leq Ch^2 \|\partial_t E\|_{L^1(H^1)}^2 + \frac{1}{28} \max_{0 \leq k < N} \mathcal{E}_h(\xi_h^k, \xi_h^{k+1}). \end{aligned}$$

Let us note that the appearance of the projection $\widetilde{\Pi}_h$ in the residual $r_{h,p}^k$ was essential here, in order to be able to apply Lemma 4.8.

Conclusion. By summation of all the individual estimates for the respective residuals and application of Lemma 4.10, we finally obtain

$$\mathcal{E}(\xi_h^n, \xi_h^{n+1}) \leq \mathcal{E}(\xi_h^0, \xi_h^1) + 2 \left(7 \cdot \frac{1}{28} \max_{0 \leq k < N} \mathcal{E}(\xi_h^k, \xi_h^{k+1}) + C(E)h^2 + C'(E)\tau^2 \right).$$

Taking the maximum over all n , using (9), and the bound (13) for $\mathcal{E}(\xi_h^0, \xi_h^1)$, we thus obtain the required estimates for the discrete error component. By combination with the interpolation error estimate, we arrive at the estimate of Theorem 3.2. \square

Estimate of Theorem 3.3. We now split the corresponding error by

$$E(t^n) - \widetilde{\Pi}_h E_h^n = -(\widetilde{\Pi}_h E(t^n) - E(t^n)) + (\widetilde{\Pi}_h E(t^n) - \widetilde{\Pi}_h E_h^n) =: -\eta^n + \widetilde{\xi}_h^n$$

The first term is the same as before, and for the discrete error, we can use the following arguments: By the commuting diagram property of the projectors, we see that $\operatorname{curl} \widetilde{\xi}_h^n = \operatorname{curl} \xi_h^n$, which allows using the bounds of the previous proof to handle the curl-terms in the estimate of the discrete error $\widetilde{\xi}_h^n$. For the L^2 -terms, we use

$$\begin{aligned} \|\partial_\tau \widetilde{\xi}_h^{n+1/2}\|_{L^2} &= \|\widetilde{\Pi}_h (\Pi_h \partial_\tau E^{n+1/2} - \partial_\tau E_h^{n+1/2})\|_{L^2} \leq C \|\Pi_h \partial_\tau E^{n+1/2} - \partial_\tau E_h^{n+1/2}\|_{L^2} \\ &\leq C (\|\widetilde{\Pi} \partial_\tau E^{n+1/2} - \partial_\tau E_h^{n+1/2}\|_{L^2} + \|\Pi_h \partial_\tau E^{n+1/2} - \widetilde{\Pi}_h \partial_\tau E^{n+1/2}\|_{L^2}). \end{aligned}$$

In the first inequality, we made use of the bound $\|\widetilde{\Pi}_h v_h\|_{L^2} \leq C \|v_h\|_{L^2}$, which follows by the usual scaling arguments. The first term in the above estimate only involves the discrete error $\partial_\tau \xi_h^{n+1/2} = \widetilde{\Pi} \partial_\tau E^{n+1/2} - \partial_\tau E_h^{n+1/2}$, which was already analyzed

before, and the second term can be bounded by the interpolation error estimates for the two projectors. This then already yields the estimate of Theorem 3.3. \square

5. ALGEBRAIC PROPERTIES

We now discuss the implementation of the proposed methods and the algebraic properties stated in Theorems 3.2 and 3.3. Let us recall the basis functions

$$\Phi_{ij} = \lambda_i \nabla \lambda_j \quad \text{and} \quad \Phi_{ji} = -\lambda_j \nabla \lambda_i$$

associated with the edges $e_{ij} \in \mathcal{E}_h$. By basic computations, one can see the following.

Lemma 5.1. *Let $v_h = \sum_{e_{ij}} \mathbf{v}_{ij} \Phi_{ij} + \mathbf{v}_{ji} \Phi_{ji} \in V_h$ be given. Then*

$$\tilde{\Pi}_h v_h = \sum_{e_{ij} \in \mathcal{E}_h \setminus \tilde{\mathcal{E}}_h} \mathbf{v}_{ij} \Phi_{ij} + \mathbf{v}_{ji} \Phi_{ji} + \sum_{e_{ij} \in \tilde{\mathcal{E}}_h} \frac{1}{2} (\mathbf{v}_{ij} + \mathbf{v}_{ji}) (\Phi_{ij} + \Phi_{ji}).$$

Hence $\tilde{\Pi}_h v_h = \sum_{e_{ij} \in \mathcal{E}_h} \hat{\mathbf{v}}_{ij} \Phi_{ij} + \hat{\mathbf{v}}_{ji} \Phi_{ji}$ with coefficients given by $\hat{\mathbf{v}}_{ij} := \mathbf{v}_{ij}$, $\hat{\mathbf{v}}_{ji} := \mathbf{v}_{ji}$ for the edges $e_{ij} \in \mathcal{E}_h \setminus \tilde{\mathcal{E}}_h$ and $\hat{\mathbf{v}}_{ij} = \hat{\mathbf{v}}_{ji} := \frac{1}{2} (\mathbf{v}_{ij} + \mathbf{v}_{ji})$ for the edges $e_{ij} \in \tilde{\mathcal{E}}_h$.

For the following considerations, we always assume that the degrees of freedom are sorted edge-wise. This allows us to make the following statements.

Lemma 5.2. *The equation (4) is equivalent to the algebraic system (5) with*

$$\begin{aligned} [\mathbf{M}_{\varepsilon+\tau\sigma/2}]_{ij,kl} &= \langle (\varepsilon + \tau\sigma/2) \Phi_{kl}, \Phi_{ij} \rangle_h, & [\mathbf{f}^n]_{ij} &= \langle f(t^n), \Phi_{ij} \rangle, \\ [\mathbf{K}_\nu]_{ij,kl} &= \langle \nu \operatorname{curl} \Phi_{kl}, \operatorname{curl} \Phi_{ij} \rangle, & [\mathbf{g}^n]_{ij} &= \langle g(t^n), \Phi_{ij} \rangle_{\partial\Omega}. \end{aligned}$$

Both matrices are sparse, and $\mathbf{M}_{\varepsilon+\tau\sigma/2}$ is block diagonal, with one block per vertex of the mesh coupling all degrees of freedom not vanishing at this vertex. Furthermore

$$\hat{\mathbf{M}}_\sigma = \mathbf{Q}^\top \mathbf{M}_\sigma \mathbf{Q} \quad \text{with} \quad [\mathbf{M}_\sigma]_{ij,kl} = (\sigma \Phi_{kl}, \Phi_{ij})_h,$$

and the projection matrix \mathbf{Q} is block diagonal with 2×2 blocks of the form

$$\frac{1}{2} \begin{pmatrix} 1 & 1 \\ 1 & 1 \end{pmatrix} \quad \text{and} \quad \begin{pmatrix} 1 & 0 \\ 0 & 1 \end{pmatrix}$$

for the edges $e_{ij} \in \tilde{\mathcal{E}}_h$ and $e_{ij} \in \mathcal{E}_h \setminus \tilde{\mathcal{E}}_h$, respectively.

The assertions follow immediately from the properties of the basis functions; for details, see [9, 31]. This already proves the second claim of Theorem 3.2. \square

Algebraic reduction. We next derive the reduced scheme (6). To do so, we start with the following observation, which again follows from elementary arguments.

Lemma 5.3. *The function $\tilde{\Pi}_h v_h$ can be expressed equivalently as*

$$\tilde{\Pi}_h v_h = \sum_{e_{ij} \in \mathcal{E}_h \setminus \tilde{\mathcal{E}}_h} \tilde{\mathbf{v}}_{ij} \Phi_{ij} + \tilde{\mathbf{v}}_{ji} \Phi_{ji} + \sum_{e_{ij} \in \tilde{\mathcal{E}}_h} \tilde{\mathbf{v}}_{ij} \tilde{\Phi}_{ij}, \quad \tilde{\Phi}_{ij} = \Phi_{ij} + \Phi_{ji},$$

with $\tilde{\mathbf{v}}_{ij} = \mathbf{v}_{ij}$, $\tilde{\mathbf{v}}_{ji} = \mathbf{v}_{ji}$ for $e_{ij} \in \mathcal{E}_h \setminus \tilde{\mathcal{E}}_h$ and $\tilde{\mathbf{v}}_{ij} = \frac{1}{2} (\mathbf{v}_{ij} + \mathbf{v}_{ji})$ for $e_{ij} \in \tilde{\mathcal{E}}_h$, and the collection $\{\Phi_{ij}, \Phi_{ji} : e_{ij} \in \mathcal{E}_h \setminus \tilde{\mathcal{E}}_h\} \cup \{\tilde{\Phi}_{ij} := \Phi_{ij} + \Phi_{ji} : e_{ij} \in \tilde{\mathcal{E}}_h\}$ is a basis for \tilde{V}_h .

Also for the reduced space, the degrees of freedom are sorted edgewise. Then the relation between the coefficients \mathbf{v}_{ij} , $\hat{\mathbf{v}}_{ij}$ and $\tilde{\mathbf{v}}_{ij}$ can be expressed as follows.

Lemma 5.4. *Let \mathbf{P} be the block-diagonal (prolongation) matrix with blocks*

$$\begin{pmatrix} 1 \\ 1 \end{pmatrix} \quad \text{and} \quad \begin{pmatrix} 1 & 0 \\ 0 & 1 \end{pmatrix}$$

for edges $e_{ij} \in \tilde{\mathcal{E}}_h$ and $e_{ij} \in \mathcal{E}_h \setminus \tilde{\mathcal{E}}_h$, respectively. Then $\mathbf{Q} = \mathbf{P}(\mathbf{P}^\top \mathbf{P})^{-1} \mathbf{P}^\top$ and $\mathbf{P}^\top \mathbf{P}$ is diagonal with entries $1/2$ and 1 , respectively. Furthermore,

$$\hat{\mathbf{v}} = \mathbf{P} \tilde{\mathbf{v}} \quad \text{and} \quad \tilde{\mathbf{v}} = \mathbf{R} \mathbf{v} \quad \text{with} \quad \mathbf{R} = (\mathbf{P}^\top \mathbf{P})^{-1} \mathbf{P}^\top.$$

This lemma allows us to express the coefficients of $\tilde{\Pi}_h v_h$ in the basis of \tilde{V}_h by the coefficients of the expansion in the basis of V_h . With the help of this result, we can now derive the algebraic form (6) of the reduced scheme of Theorem 3.3.

Lemma 5.5. *Let $(\mathbf{E}^n)_n$ be a solution of (5). Then $\tilde{\mathbf{E}}^n = \mathbf{R} \mathbf{E}^n$ satisfies (6) with*

$$\tilde{\mathbf{M}}_{\varepsilon+\tau\sigma/2}^{-1} = \mathbf{R} \mathbf{M}_{\varepsilon+\tau\sigma/2}^{-1} \mathbf{R}^\top, \quad \tilde{\mathbf{M}}_\sigma = \mathbf{P}^\top \mathbf{M}_\sigma \mathbf{P}, \quad \tilde{\mathbf{K}}_\nu = \mathbf{P}^\top \mathbf{K}_\nu \mathbf{P}$$

and right-hand sides

$$\tilde{\mathbf{F}}^n = \mathbf{R} \mathbf{M}_{\varepsilon+\tau\sigma/2}^{-1} \mathbf{f}^n \quad \tilde{\mathbf{G}}^n = \mathbf{R} \mathbf{M}_{\varepsilon+\tau\sigma/2}^{-1} \mathbf{g}^n, \quad (14)$$

where $\mathbf{f}^n, \mathbf{g}^n$ are defined as in Lemma 5.2. Hence, the projection $\tilde{E}_h^n = \tilde{\Pi}_h E_h^n$ of the solution of Method 3.1 is given by (6).

Proof. Since $\mathbf{M}_{\varepsilon+\tau\sigma/2}$ is regular, the scheme (5) is equivalent to

$$\partial_{\tau\tau} \mathbf{E}^n = \mathbf{M}_{\varepsilon+\tau\sigma/2}^{-1} \left(-\hat{\mathbf{M}}_\sigma \partial_\tau \mathbf{E}^{n-1/2} - \mathbf{K}_\nu \mathbf{E}^n + \mathbf{f}^n + \mathbf{g}^n \right).$$

We further multiply this equation from the left by $\mathbf{R}^\top = \mathbf{P}(\mathbf{P}^\top \mathbf{P})^{-1}$ and note that $\mathbf{P} \mathbf{R} = \mathbf{P}(\mathbf{P}^\top \mathbf{P})^{-1} \mathbf{P}^\top = \mathbf{Q}$, which follows from the definition of the matrices. We see

$$\hat{\mathbf{M}}_\sigma = \mathbf{R}^\top \mathbf{P}^\top \mathbf{M}_\sigma \mathbf{P} \mathbf{R} \quad \text{and} \quad \mathbf{K}_\nu = \mathbf{Q}^\top \mathbf{K}_\nu \mathbf{Q} = \mathbf{R}^\top \tilde{\mathbf{K}}_\nu \mathbf{R},$$

where we used the algebraic form of the commuting diagram property of the projection $\tilde{\Pi}_h$, see (8). Using the definitions of $\tilde{\mathbf{E}}^n, \tilde{\mathbf{F}}^n$, and $\tilde{\mathbf{G}}^n$, we thus conclude that

$$\begin{aligned} \partial_{\tau\tau} \tilde{\mathbf{E}}^n &= \partial_{\tau\tau} \mathbf{R} \mathbf{E}^n = \mathbf{R} \mathbf{M}_{\varepsilon+\tau\sigma/2}^{-1} \left(-\mathbf{R}^\top \tilde{\mathbf{M}}_\sigma \mathbf{R} \partial_\tau \mathbf{E}^{n-1/2} - \mathbf{R}^\top \tilde{\mathbf{K}}_\nu \mathbf{R} \mathbf{E}^n + \mathbf{f}^n + \mathbf{g}^n \right) \\ &= \tilde{\mathbf{M}}_{\varepsilon+\tau\sigma/2}^{-1} \left(-\tilde{\mathbf{M}}_\sigma \partial_\tau \tilde{\mathbf{E}}^{n-1/2} - \tilde{\mathbf{K}}_\nu \tilde{\mathbf{E}}^n \right) + \tilde{\mathbf{F}}^n + \tilde{\mathbf{G}}^n \end{aligned}$$

This already yields the algebraic form given in (6) and concludes the proof. \square

Remark 5.6. The choice (14) for the right-hand sides $\tilde{\mathbf{F}}^n, \tilde{\mathbf{G}}^n$ in the reduced method makes use of the vectors $\mathbf{f}^n, \mathbf{g}^n$ with two degrees of freedom for each edge. An alternative and more direct choice would be

$$\tilde{\mathbf{F}}^n := \tilde{\mathbf{M}}_{\varepsilon+\tau\sigma/2}^{-1} \tilde{\mathbf{f}}^n \quad \text{and} \quad \tilde{\mathbf{G}}^n := \tilde{\mathbf{M}}_{\varepsilon+\tau\sigma/2}^{-1} \tilde{\mathbf{g}}^n, \quad (15)$$

which now only depends on the vectors $\tilde{\mathbf{f}}^n$ and $\tilde{\mathbf{g}}^n$ assembled on the reduced finite element space \tilde{V}_h . This modification can be included in our analysis, if one replaces assumption (A5) by choosing $\tilde{\mathcal{E}}_h \subset \mathcal{E}_h$ such that

(A5*) σ and f are continuous across edges $e \in \tilde{\mathcal{E}}_h$ lying in the interior Ω , and $\sigma = 0, g = 0$ for all edges $e \in \tilde{\mathcal{E}}_h$ on the boundary $\partial\Omega$.

This allows us to apply a variant of Lemma 4.8 which covers the additional consistency error introduced by the representation of f ; the boundary term g is already fully covered by the original assumption (A5) since it vanishes along all edges where no reduction is applied. The time-stepping scheme resulting from this modified choice of the right-hand sides can be stated as

$$\partial_{\tau\tau}\tilde{\mathbf{E}}^n = \tilde{\mathbf{M}}_{\varepsilon+\tau\sigma/2}^{-1}(-\tilde{\mathbf{M}}_{\sigma}\partial_{\tau}\tilde{\mathbf{E}}^{n-1/2} - \tilde{\mathbf{K}}_{\nu}\tilde{\mathbf{E}}^n + \tilde{\mathbf{f}}^n + \tilde{\mathbf{g}}^n), \quad (16)$$

and used as an alternative to (6). In our numerical tests, we will compare the two versions (6) and (16), in particular, also highlighting the importance of the additional conditions in assumption (A5*) for the latter.

6. NUMERICAL VALIDATION

As a model problem for our numerical tests, we consider the scattering of a plane electromagnetic wave from a cylinder. Under the usual symmetry assumptions, this can be modeled by Maxwell's equations in two space dimensions. All results from the three-dimensional setting translate almost verbatim. The main differences are that \mathcal{T}_h now corresponds to a triangular mesh and that the space \tilde{V}_h is a subspace of $P_1(K)^2 \cap H(\text{curl}; \Omega)$. Moreover, the triangular vertex rule

$$(a, b)_h = \sum_T \frac{|T|}{3} \sum_{v_i \in T} a(v_i) \cdot b(v_i)$$

is used for the numerical quadrature.

Model problem. The geometric setup of our test problem is illustrated in Figure 1. The computational domain $\Omega = (-1, 1)^2$ is split into two parts: The circular region Ω_S of radius $r_S = 0.3$ contains the scatterer with material parameters $\varepsilon = \nu = 1$ and $\sigma = 100$. For the surrounding medium $\Omega \setminus \Omega_S$ we take $\varepsilon = \nu = 1$ and $\sigma = 0$.

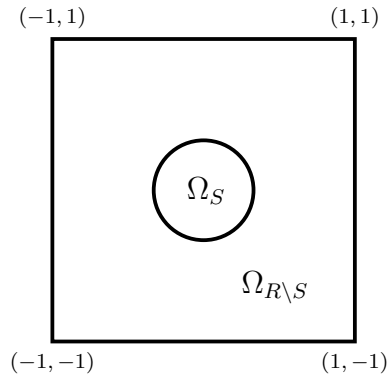


FIGURE 1. Computational domain for the wave scattering problem.

Test scenario. For excitation of the fields, the initial and boundary conditions are chosen to match the corresponding traces of the plane wave

$$\tilde{E}(x, y, t) = \begin{pmatrix} -k_2 \\ k_1 \end{pmatrix} a(k_1 x + k_2 y - t)$$

with envelope $a(x) = 2e^{-10(x+3)^2}$ and $k = (k_1, k_2) = \frac{1}{\sqrt{2}}(1, 1)$. The function \tilde{E} satisfies (1)–(2) with $\varepsilon = \nu = 1$, $\sigma = 0$, and data $f = 0$ and $g = n \times (\nu \text{curl } \tilde{E})$. As a

consequence, the plane wave will first propagate freely through $\Omega \setminus \Omega_S$, but then get scattered at the inclusion Ω_S with high conductivity. The scattered wave will then travel back through the free region $\Omega \setminus \Omega_S$ and finally be artificially reflected at the outer boundary $\partial\Omega$. In Figure 2, some corresponding snapshots of the numerical solution $E_h(t)$ are depicted.

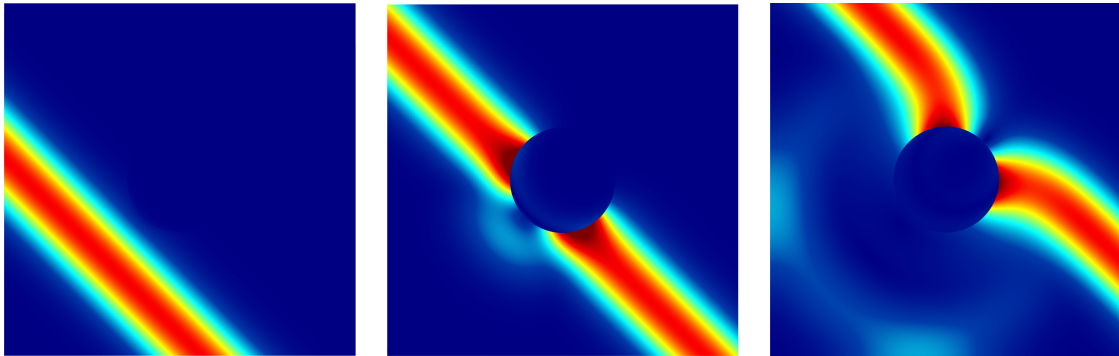


FIGURE 2. Absolute values of the simulated electric field $E_h(t)$ at time $t = 1.5$ (left), $t = 2$ (middle), and $t = 2.5$ (right).

Discretization setup. To examine the convergence of the methods, we consider a sequence of meshes \mathcal{T}_h obtained by uniform refinement of an initial unstructured coarse mesh. The time step τ is chosen following the CFL condition (A4). Let us note that σ is continuous everywhere but on the edges along $\partial\Omega_S$ and vanishes on the outer boundary $\partial\Omega$. To illustrate our theoretical results, we consider Method 3.1 for three different choices of $\tilde{\mathcal{E}}_h$, namely

- $\tilde{\mathcal{E}}_h = \emptyset$: This leads to $\tilde{V}_h = \mathcal{NC}_1$ with two degrees of freedom for every edge;
- $\tilde{\mathcal{E}}_h \subseteq \mathcal{E}_h$ such that (A5) is satisfied, i.e. $\mathcal{N}_0 \subset \tilde{V}_h \subset \mathcal{NC}_1$: in particular, only one degree of freedom is used for all edges not lying on the boundary $\partial\Omega_S$;
- $\tilde{\mathcal{E}}_h = \mathcal{E}_h$: This amounts to $\tilde{V}_h = \mathcal{N}_0$ and violates assumption (A5).

The corresponding finite element solutions are denoted by $E_h^{\mathcal{NC}}$, $E_h^{\mathcal{N}^+}$ and $E_h^{\mathcal{N}}$. For measuring the error between two functions E_h and E_h^* , we use

$$\| \| E_h - E_h^* \| \| := \frac{\| \partial_\tau (E_h - E_h^*) \|_{\ell_\infty(L^2(\Omega))}}{\| \partial_\tau E_h^* \|_{\ell_\infty(L^2(\Omega))}} + \frac{\| \text{curl}(\hat{E}_h - \hat{E}_h^*) \|_{\ell_\infty(L^2(\Omega))}}{\| \text{curl} \hat{E}_h^* \|_{\ell_\infty(L^2(\Omega))}}$$

Computational results. We first study the error and convergence rate of the \mathcal{NC}_1 method. Since the exact solution to our model problem is somewhat cumbersome to compute, we estimate the discretization errors by comparing the numerical solutions obtained on two different nested meshes. As one can infer from Table 1, first-order convergence of the \mathcal{NC}_1 -method is observed, which is in perfect agreement with our previous studies [9, 31].

In the following tests, we evaluate the convergence rates for the \mathcal{N}_0^+ and \mathcal{N}_0 methods by comparing them to the simulations obtained with the \mathcal{NC}_1 method. For the \mathcal{N}_0^+ -method, assumption (A5) is valid, and we observe first-order convergence as predicted by our theoretical results. Recall that this method has two degrees of freedom (only) for all edges at the interface $\partial\Omega_S$ where σ has a jump. The \mathcal{N}_0 -method,

$h \approx$	$\ \ E_h^{\mathcal{N}^c} - E_{2h}^{\mathcal{N}^c} \ \ $	eoc	dofs
2^{-3}	0.779603	—	2.296
2^{-4}	0.373586	1.06	9.056
2^{-5}	0.185312	1.01	35.968
2^{-6}	0.093906	0.98	143.360
2^{-7}	0.046257	1.02	572.416
2^{-8}	0.023158	1.00	2.287.616
2^{-9}	0.011612	1.00	9.146.368

TABLE 1. Errors, the estimated order of convergence (eoc) and the number of degrees of freedom (dofs) for a multitude of mesh sizes h with fixed time step sizes $\tau = 0.28 h$.

$h \approx$	$\ \ E_h^{\mathcal{N}^+} - E_h^{\mathcal{N}^c} \ \ $	eoc	dofs	$\ \ E_h^{\mathcal{N}} - E_h^{\mathcal{N}^c} \ \ $	eoc	dofs
2^{-3}	0.098385	—	1.164	0.105887	—	1.148
2^{-4}	0.049076	1.00	4.560	0.053302	1.00	4.528
2^{-5}	0.024133	1.02	18.048	0.027561	0.95	17.984
2^{-6}	0.011923	1.01	71.808	0.015084	0.87	71.680
2^{-7}	0.005916	1.01	286.464	0.008739	0.79	286.208
2^{-8}	0.002945	1.00	1.144.320	0.005371	0.70	1.143.808
2^{-9}	0.001469	1.00	4.574.208	0.003474	0.63	4.573.184

TABLE 2. Errors, the estimated order of convergence (eoc) and the number of degrees of freedom (dofs) for a multitude of mesh sizes h with fixed time step sizes $\tau = 0.28 h$.

on the other hand, uses algebraic reduction also at the interface, thus violating assumption (A5). This indeed results in a reduction of the convergence rate, as could be expected from our analysis. Condition (A5) therefore seems necessary to obtain the optimal convergence rates in the presence of discontinuous conductivities. In further tests, we also verified that assumption (A5*) is necessary if the right-hand sides are chosen according to (15).

Additional consistency errors. To better understand the convergence breakdown when violating the consistency conditions (A5) and (A5*), we illustrate in Figure 3 the local contributions of the errors $\| \| E_h^{\mathcal{N}} - E_h^{\mathcal{N}^c} \| \|$ for $h = 2^{-4}$ for the two choices (14) and (15) of the right-hand sides. As can be expected, the dominating error contributions come from the interface and the boundary, where the consistency conditions (A5) respectively (A5*) are violated.

Inspection of the CFL condition. As we have observed in assumption (A4), the CFL condition is somewhat non-standard, introducing an additional term depending on the projection $\tilde{\Pi}_h$. To illustrate the effect of this additional term, we compute the largest time step $\tau = \tau_{\max}$ for which

$$\frac{\tau_{\max}^2}{4} \mathbf{v}^\top \mathbf{K}_\nu \mathbf{v} - \frac{1}{2} \mathbf{v}^\top \mathbf{M}_\varepsilon \mathbf{v} + \gamma \frac{\tau_{\max}}{2} \left| \mathbf{v}^\top \left(\widehat{\mathbf{M}}_\sigma - \mathbf{M}_\sigma \right) \mathbf{v} \right| \geq 0$$

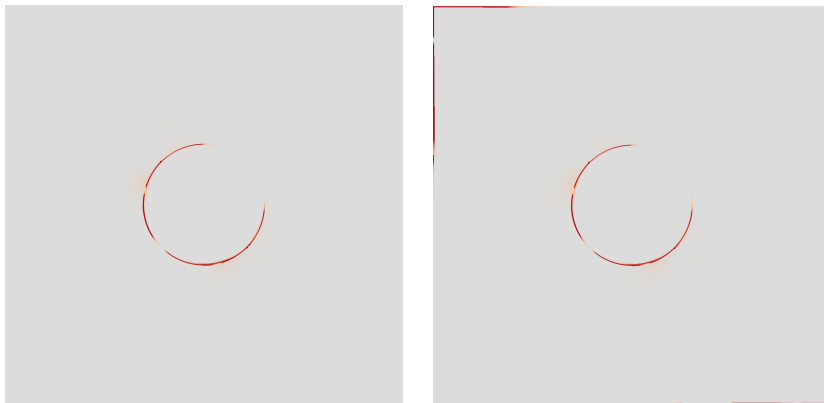


FIGURE 3. Local contributions of the error $\|E_h^{\mathcal{N}} - E_h^{\mathcal{NC}}\|$ for $h = 2^{-4}$ with different implementations of the right-hand sides. The red color indicates which part of the mesh the error dominates.

for all vectors \mathbf{v} , where $\gamma = 0$ for the \mathcal{NC}_1 method and $\gamma = 1$ for the \mathcal{N}_0^+ method. By Taylor expansion, we note that τ_{\max} behaves approximately like

$$\tau_{\max} \sim \sqrt{\frac{\varepsilon}{\nu}} h + \gamma \frac{\sigma}{2\nu} h^2. \quad (17)$$

For $\gamma = 0$ or $\sigma = 0$, we obtain the classic linear dependence $\tau \leq Ch$. In Table 3, we display the values of $C = \tau_{\max}/h$ for each of the methods for the model parameters used in our simulations. First note that the CFL constant C is uniformly bounded

h	\mathcal{NC}_1	\mathcal{N}_0^+
2^{-3}	0.391076	0.210000
2^{-4}	0.381624	0.317041
2^{-5}	0.377977	0.377977
2^{-6}	0.376846	0.376846
2^{-7}	0.376528	0.376528

TABLE 3. CFL constants for both the \mathcal{NC}_1 and the \mathcal{N}_0^+ method on a sequence of uniformly refined meshes.

from above for both methods. While for larger values of h , the CFL constant is somewhat more stringent for the \mathcal{N}_0^+ method, the constant C behaves almost the same for small h , which is in perfect agreement with (17). The algebraic reduction hence does not have a severe effect on the maximal admissible time step.

7. DISCUSSION

In this paper, we proposed and analyzed finite-element schemes which can be seen as a natural extension of the Yee scheme to unstructured grids and inhomogeneous lossy media. While the number of degrees of freedom can be reduced to one for almost all edges, the necessity incorporation of two degrees of freedom at interfaces or boundaries with material jumps has been illustrated. A full convergence analysis of the schemes could be provided and optimal convergence could be proven under reasonable assumptions. Alternative extensions of the Yee scheme to triangular and

tetrahedral elements based on dual cell complexes have been proposed previously in [4, 5, 19]. While in some settings, the algebraic form of these methods is similar or even identical to ours, the constructions in these papers follow a rather geometric approach which complicates the error analysis. The results obtained in our paper may be useful to gain further insight also into these related methods.

REFERENCES

- [1] D. Boffi, F. Brezzi, and M. Fortin. *Mixed finite element methods and applications*, volume 44 of *Springer Series in Computational Mathematics*. Springer, Heidelberg, 2013.
- [2] A. Bossavit and L. Kettunen. Yee-like schemes on a tetrahedral mesh, with diagonal lumping. *Int. J. Numer. Model.*, 12:129–142, 1999.
- [3] S. C. Brenner and L. R. Scott. *The mathematical theory of finite element methods*, volume 15 of *Texts in Applied Mathematics*. Springer, New York, third edition, 2008.
- [4] L. Codecasa, B. Kapidani, R. Specogna, and F. Trevisan. Novel FDTD technique over tetrahedral grids for conductive media. *IEEE Transactions on Antennas and Propagation*, 66:5387–5396, 2018.
- [5] L. Codecasa and M. Politi. Explicit, consistent, and conditionally stable extension of FDTD to tetrahedral grids by FIT. *IEEE Transactions on Magnetics*, 44:1258–1261, 2008.
- [6] G. Cohen. *Higher-Order Numerical Methods for Transient Wave Equations*. Springer, Heidelberg, 2002.
- [7] G. Cohen and P. Monk. Efficient edge finite element schemes in computational electromagnetism. In *Mathematical and numerical aspects of wave propagation*, pages 250–259. SIAM, Philadelphia, PA, 1995.
- [8] G. Cohen and S. Pernet. *Finite Element and Discontinuous Galerkin Methods for Transient Wave Equations*. Scientific Computation. Springer Netherlands, 2016.
- [9] H. Egger and B. Radu. A mass-lumped mixed finite element method for Maxwell’s equations. In *Scientific computing in electrical engineering*, volume 32 of *Math. Ind.*, pages 15–24. Springer, Cham, 2020.
- [10] H. Egger and B. Radu. A second-order finite element method with mass lumping for Maxwell’s equations on tetrahedra. *SIAM J. Numer. Anal.*, 59:864–885, 2021.
- [11] A. Elm kies and P. Joly. Éléments finis d’arête et condensation de masse pour les équations de Maxwell: le cas 2D. *Comptes Rendus de l’Académie des Sciences - Series I - Mathematics*, 324:1287–1293, 1997.
- [12] A. Elm kies and P. Joly. Éléments finis d’arête et condensation de masse pour les équations de Maxwell: le cas de dimension 3. *Comptes Rendus de l’Académie des Sciences - Series I - Mathematics*, 325:1217–1222, 1997.
- [13] A. Ern and J.-L. Guermond. *Theory and practice of finite elements*, volume 159 of *Applied Mathematical Sciences*. Springer-Verlag, New York, 2004.
- [14] R. Farwig and V. Rosteck. Note on Friedrichs’ inequality in N -star-shaped domains. *J. Math. Anal. Appl.*, 435:1514–1524, 2016.
- [15] S. Geever, W. Mulder, and J. van der Vegt. New higher-order mass-lumped tetrahedral elements for wave propagation modelling. *SIAM Journal on Scientific Computing*, 40:A2830–A2857, 2018.
- [16] J. S. Hesthaven and T. Warburton. *Nodal discontinuous Galerkin methods*, volume 54 of *Texts in Applied Mathematics*. Springer, New York, 2008. Algorithms, analysis, and applications.
- [17] R. Holland. Finite-difference solution of Maxwell’s equations in generalized nonorthogonal coordinates. *IEEE Trans. on Nuclear Science*, NS-30:4589–4591, 1983.
- [18] P. Joly. Variational methods for time-dependent wave propagation problems. In *Topics in Computational Wave Propagation*, volume 31 of *LNCSE*, pages 201–264. Springer, 2003.
- [19] B. Kapidani, L. Codecasa, and J. Schöberl. An arbitrary-order Cell Method with block-diagonal mass-matrices for the time-dependent 2D Maxwell equations. *J. Comput. Phys.*, 433:Paper No. 110184, 20, 2021.

- [20] J. F. Lee, R. Pandalech, and R. Mittra. Modeling three-dimensional discontinuities in waveguides using nonorthogonal FDTD algorithm. *IEEE Trans. on Microwave Theory and Techniques*, 40:346–352, 1992.
- [21] R. Leis. *Initial Boundary Value Problems in Mathematical Physics*. John Wiley, New York, 1988.
- [22] C. G. Makridakis and P. Monk. Time-discrete finite element schemes for Maxwell’s equations. *RAIRO Modél. Math. Anal. Numér.*, 29:171–197, 1995.
- [23] P. Monk. Analysis of a finite element methods for Maxwell’s equations. *SIAM J. Numer. Anal.*, 29:714–729, 1992.
- [24] P. Monk. A comparison of three mixed methods for the time-dependent Maxwell’s equations. *SIAM J. Sci. Statist. Comput.*, 13:1097–1122, 1992.
- [25] P. Monk. An analysis of Nédélec’s method for the spatial discretization of Maxwell’s equations. *J. Comput. Appl. Math.*, 47:101–121, 1993.
- [26] P. Monk. Finite element time domain methods for Maxwell’s equations. In *Second International Conference on Mathematical and Numerical Aspects of Wave Propagation (Newark, DE, 1993)*, pages 380–389. SIAM, Philadelphia, PA, 1993.
- [27] P. Monk. *Finite element methods for Maxwell’s equations*. Numerical Mathematics and Scientific Computation. Oxford University Press, New York, 2003.
- [28] P. B. Monk and E. Süli. A convergence analysis of Yee’s scheme on nonuniform grids. *SIAM J. Numer. Anal.*, 31:393–412, 1994.
- [29] J. C. Nédélec. A new family of mixed finite elements in \mathbb{R}^3 . *Numer. Math.*, 50:57–81, Jan 1986.
- [30] J. C. Nédélec. Mixed finite elements in \mathbb{R}^3 . *Numer. Math.*, 35:315–341, 1980.
- [31] B. Radu. *Finite element mass lumping for $H(\text{div})$ and $H(\text{curl})$* . PhD thesis, Technische Universität Darmstadt, Darmstadt, 2022.
- [32] R. Schuhmann and T. Weiland. FDTD on nonorthogonal grids with triangular fillings. *IEEE Trans. Magn.*, pages 1470–1473, 1998.
- [33] R. Schuhmann and T. Weiland. A stable interpolation technique for FDTD on nonorthogonal grids. *Int. J. Numer. Model.*, 11:299–306, 1998.
- [34] A. Taflove. Application of the finite-difference time-domain method to sinusoidal steady-state electromagnetic-penetration problems. *IEEE Transactions on Electromagnetic Compatibility*, EMC-22:191–202, Aug 1980.
- [35] A. Taflove and S. C. Hagness. *Computational electrodynamics: the finite-difference time-domain method*. Artech House, Norwood, 3rd edition, 2005.
- [36] T. Weiland. A discretization model for the solution of Maxwell’s equations for six-component fields. *Archiv Elektronik und Uebertragungstechnik*, 31:116–120, Mar. 1977.
- [37] T. Weiland. Finite integration method and discrete electromagnetism. In P. Monk, C. Carstensen, S. Funken, W. Hackbusch, and R. H. W. Hoppe, editors, *Computational Electromagnetics*, pages 183–198, Berlin, Heidelberg, 2003. Springer Berlin Heidelberg.
- [38] K. Yee. Numerical solution of initial boundary value problems involving Maxwell’s equations in isotropic media. *IEEE Transactions on Antennas and Propagation*, 14:302–307, May 1966.